ELECTRONIC STRUCTURE AND THERMODYNAMIC PROPERTIES OF LI-ION INSERTION IN SULFONAMIDES COMPOUNDS AS ORGANIC HIGH-ENERGY DENSITY CATHODES

Dissertation in partial fulfillment of the requirements for the degree of

MASTER OF SCIENCE IN MATERIALS PHYSICS

UPPSALA
UNIVERSITET

Uppsala University
Department of Physics and Astronomy

Mirna Alhanash

[August 2021]

ELECTRONIC STRUCTURE AND THERMODYNAMIC PROPERTIES OF LI-ION INSERTION IN SULFONAMIDES COMPOUNDS AS ORGANIC HIGH-ENERGY DENSITY CATHODES

Dissertation in partial fulfillment of the requirements for the degree of

MASTER OF SCIENCE WITH A MAJOR IN MATERIALS PHYSICS

Uppsala University
Department of Physics and Astronomy

Approved by

Supervisor, Assoc. Prof. C. Moyses Araujo

Topic Reviewer, Professor Olle Eriksson

Examiner, Assoc. Prof. Andreas Korn

[August 2021]

Acknowledgment

I would first like to thank my supervisor, Dr. C. Moyses Araujo, for his invaluable guidance throughout my master's journey from the early formulation of the research in previous projects building up to the thesis. His insightful feedback helped me better understand the research realm of looking through the literature, finding patterns, and understanding data. His kindness and constant support will forever be treasured. I would also like to thank the Ph.D. student in the research group who helped and mentored me throughout the research as well, Rodrigo P. Carvalho, who was always ready to answer all the questions I had, as well as explain important concepts and give valuable advice.

In addition, I would like to thank my family for always supporting me and for their unconditional love, I am who I am today because of them. I would also like to extend my gratitude to my friends for their precious support and for always making my heart full.
Finally, to the curious-minded non-scientist who always explained big concepts in simple logical ways my father, Dib Alhanash, who saw this work started and supported me throughout it but did not live to see it finished, this is dedicated to you.

Abstract

The world's ever-growing energy demand has evoked great interest in exploring renewable energy sources along with sustainable energy storage systems. While inorganic physics of rocking chair mechanism used in Li-ion battery have proven to provide high energy density and high performance, there are problems yet to be overcome in terms of sustainability and recyclability. This is why research in organic batteries has been on the rise, yet the diversity of organic battery frameworks remains limited and requires overcoming multiple obstacles that restrain the performance of an all-organic battery system. A recent advance in the design of organic electrode material by Wang et al. has shown the possibility of a new stable and tunable class of conjugated sulfonamides (CSA) with an experimental voltage range between 2.85V and 3.45V [5]. A theoretical approach to study these organic materials is taken in this thesis research where the effects of such compounds on the redox potential, physics of ion insertion, and other thermodynamical properties are examined. Density Functional Theory (DFT) is employed in this investigation along with an evolutionary algorithm to generate information about the crystal structure of mentioned systems, their density of states (DOS), and charge distribution in pristine form and after lithiation. Quinone systems with oxygen groups were investigated in a previous research project that complements this thesis which looks into a quinone system with sulfonamide compounds where a comparison between the two could offer more understanding of the electrochemistry of such systems for their application in batteries as high performing organic cathode materials on a par with other inorganic materials.

Summary in Swedish

Världens ständigt växande energibehov har väckt stort intresse för att utforska förnybara energikällor tillsammans med hållbara energilagringssystem. Även om litiumjonbatterier har visat sig ge konkurrenskraftiga egenskaper och fördelar, finns det fortfarande problem som inte kan övervinnas när det gäller hållbarhet och återvinningsbarhet. Det är därför som forskningen om organiska batterier har ökat, där en nyligen framsteg i utformningen av organiskt elektrodmaterial av Wang et al. har visat möjligheten för en ny stabil och avstämbar klass av konjugerade sulfonamider (CSA) med ett experimentellt spänningsintervall mellan 2,85V och 3,45V [5]. Ett teoretiskt tillvägagångssätt för att studera dessa sulfonamider används i denna avhandlingsforskning för att förstå elektrokemi för sådana system för deras användning i batterier som högpresterande organiska katodmaterial i nivå med andra oorganiska material.

Table of Contents

1 Introduction

For the past three decades, lithium-ion batteries (LIBs) have been the most powerful and dominant technology in the battery market, catering to the gigantic growth seen recently in portable electronics. This battery technology emerged fiercely owing to its -heavily-researched- high energy density which allowed it to leapfrog over other battery systems at the time [1]. With the substantial surge of the Internet of things and portable electronics and their integration into our daily life, lithium-ion batteries powering such technologies have carved their place as indispensable products. For this reason, it comes as no surprise that the 2019 Nobel Prize award in chemistry was awarded to John B. Goodenough, M. Stanley Whittingham, and Akira Yoshino for the development of lithium-ion batteries [2].

With the world rapidly marching into the fourth industrial revolution and a higher than ever energy demand, finding and developing renewable energy sources have become a crucial research focus in order to match our increased energy consumption without completely depleting the world's resources. This means that developing appropriate energy storage systems is also of high priority in today's energy research due to its essential role in utilizing the power generated from such renewable resources and the freedom it offers to use stored energy whenever needed. Since scientists are making an effort to move away from fossil fuel sources and generate green energy to account for the extra needed energy, which is the main cause of climate change, it is only logical to develop energy storage systems that go along with such sustainable goals [3]. This, however, is where current lithium-ion battery physics reaches its limitation partially due to the use of inorganic non-abundant materials for its electrodes. The need to generate a higher energy storage capacity to match our energy needs places inorganic transition metals under the spotlight for battery cathode research, however, this comes at the expense of the thermal stability of the

battery system, sustainability, and cost. Due to mentioned limitations of the current LIBs materials, the field of organic batteries has proved to be a promising research topic that provides an alternative material type that is both environmentally sustainable and cost-effective. Using organic compounds to be used in electrochemical energy storage systems has shown to be advantageous due to the materials' abundance in the environment that cuts the cost of production and synthesis, especially if it was derived from the biomass [3]. They also have a lower carbon footprint compared to transition metals in LIBs where organic materials have an easily available recyclability route of thermal combustion that does not require the same energy needed for recycling inorganic materials. With the many advantages, organic batteries offer to the world of energy storage and the research that has been done over the years, it is yet a technology that is needed for a larger scale exploration of new materials and solutions to overcome the obstacles using such materials pose. One important factor to consider within the field of battery design is the cathode material development due to the notable effect it has on the energy density of the battery cell and its cost [1]. This is why searching for a high voltage organic cathode material is crucial to generate better battery cell results. However, there is a lack of research for such cathodes that needs to be overcome by designing new compounds along with tuning the electrochemistry of the system to provide the best possible properties to get over the energy density limitations in organic batteries.

Organic electrode materials (OEMs) have a designated classification that is based on an important quality of which all types of electrodes are typically supposed to have, which is the reversibility of the electrochemical redox reaction [6]. The contribution of the organic electrode to such redox reactions is what determines the class to which they belong. This occurs due to the shift in-charge condition of the substituent of the organic molecule that leads to storing the charge and promoting electron transportation [7]. Therefore, depending on the redox mechanism a type is categorized where a p-type (positive) represents an electron-donating material, n-type (negative) electron-accepting, and b-type (bipolar) is a combination of both types where it could undergo oxidation or reduction determined by the applied

voltage[7].

Depending on the type of organic electrode investigated, suitability to the cell material is assigned such as a Li-ion or Li-metal battery technology. This is where some limitation in the Li-ion research field appears, where the p-type electrode is commonly researched, although its anion insertion chemistry is more suitable with dual-ion cells. On the other hand, an n-type that is synthesized in an oxidated form would fit a Li-metal system better [5]. Therefore, the focus in this paper will be on the state-of-the-art reduced Li-containing n-type material. Figure [1] shows a comparison between different types of organic electrode materials (OEMs) and inorganic electrodes with respect to their specific capacity and potential where the road to discover new OEMs that are comparable to their inorganic counterparts is still ongoing.

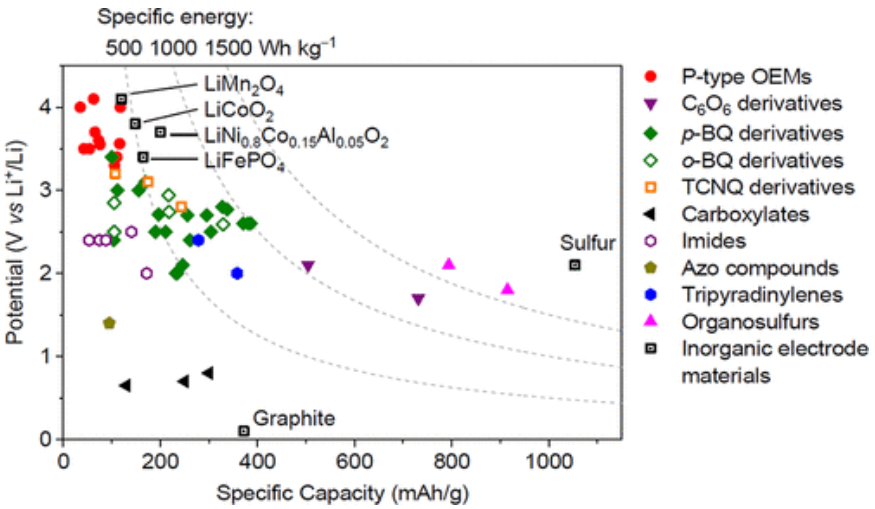

Figure [1]: A comparison between a few new OEM technologies and other inorganic electrodes regarding specific capacity and potential [8].

A typical redox reaction in an n-type material is when a transition in the organic molecule from a neutral state towards a negative one occurs due to a cation insertion shown as follow [3],

$$Organic(N) + xLi^+ + xe^- \leftrightarrow Li^+ - organic(N)^-$$

A reduction reaction occurs during the discharge cycle of an N-type material cathode, in which the organic molecule accepts an electron pair at the lowest unoccupied molecular orbital (LUMO), resulting in the formation of an anion [7]. This negative

charge is subsequently held in the organic group's conjugated backbone structure, and it is balanced by a cation such as H+, Li+, or Na+. When the material is used as a positive electrode, this reaction, as given in equation [1,] explains the discharge of the system from left to right. Because the cation uptake in an n-type material is not ion-sensitive, it can be employed with ions other than lithium. Quinones are one of the most explored n-materials [3]. Figure [2] shows examples of different classes of electrode materials along with their corresponding redox mechanisms.

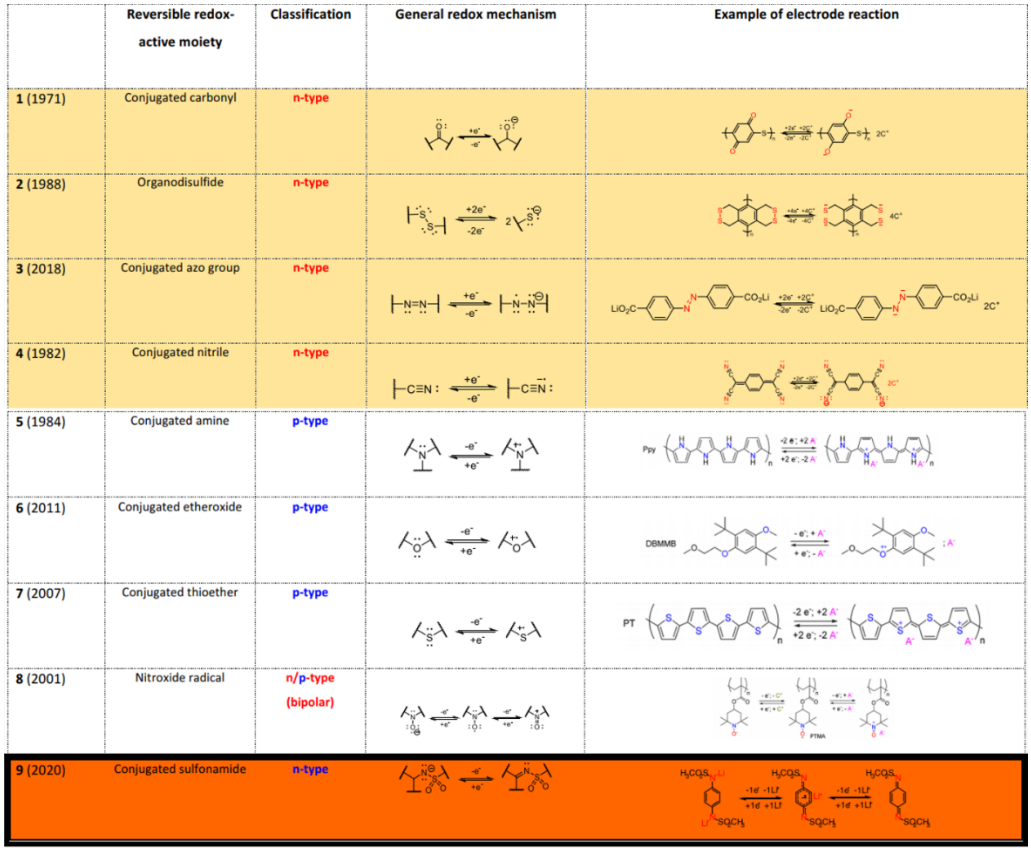

Figure [2]: A table of different organic electrode materials classes and examples with the redox mechanism and electrode reaction illustrated [5,8].

The complexity and importance of the positive electrode material research for Li-ion batteries is that while such materials need to be of high voltage and energy density, they also need an operating potential to be within the electrochemical stability window of the electrolyte. Current inorganic materials used for such cathodes, such as LiFePO4 and LiCoO2, present good electrode-electrolyte compatibility where they conveniently run above the highest unoccupied molecular orbital (HOMO) potential of the electrolyte of around 4.3 V vs. Li/Li^+ [4]. Some limitations in the battery cell

arise from such properties that need to be accommodated for; and the way to tune this limitation and obtain desired results is by utilizing the dependence of aforementioned qualities on the crystal structure of the electrode, salt layer formation, physics behind the ion insertion within the electrode structure and the redox centers electrochemistry. Finding an organic cathode material that could provide a high energy density, be compatible with the electrolyte and be stable in ambient conditions could be slightly challenging.

A newly published research paper by Wang et Al. presents a new class of conjugated sulfonamides (CSAs) used as organic cathodes with interesting qualities that are on a par with other inorganic materials like LiFePO4 [5]. This paper examines eight members of the CSA family both experimentally and theoretically showing that these compounds satisfy the requirements of the Li-ion cathode materials regarding synthesis, stability, and reversibility. They define such conditions to be that the material should be produced in the reduced Lithium held structure, stable in open air, and have a multielectron redox potential around ≥ 3V vs Li^+/Li^0 that is reversible [5]. Since these compounds comply with the mentioned prerequisites, they offer numerous advantages to be used as cathode materials where they cover a voltage range of 2.85 to 3.45V vs Li^+/Li^0 while their wide range of structural variety offers more opportunities for property tuning. These qualities bring more possibilities to the table by opening doors for future research and showing these compounds as promising candidates to be further studied. While the research on quinone systems is beneficial and hopeful, this class of CSA materials surpasses the other systems' limitations and dependence on the conjugated carbonyl redox mechanism. This thesis paper will focus on the computational analysis and further studies of three types only of conjugated sulfonamides mentioned in the original paper, shown in Figure [3].

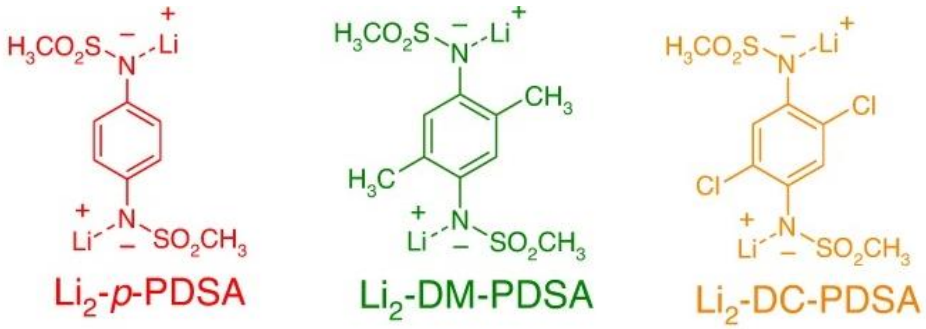

Figure [3]: dilithium 1,4-phenylenebis((methylsulfonyl)amide) Li2-p-PDSA, Dilithium (2,5-dimethyl-1,4-phenylene)bis((methylsulfonyl)amide)) Li2-DM-PDSA, (dilithium (2,5-dichloro-1,4-phenylene) bis((methylsulfonyl)amide)) Li2-DC-PDSA.

At first, a simple system (Li2-p-PDSA) is studied to bring insight to the redox center mechanisms and the general electrochemistry of the system, then a further study for larger molecules such as Li2-DM-PDSA and Li2-DC-PDSA is studied to investigate the effects of side-chain electrons on the electrochemical properties and charge distribution.

These systems will be investigated by employing Density Functional Theory (DFT) along with a genetic algorithm that will provide information about the crystal and electronic structure of the desired systems and their thermodynamical properties. This computational analysis of CSA systems that are suggested for green cathode materials could provide further insight into the materials' properties which serves as an important tool to finely tune the material to provide optimized results.

Theory

2 Theory

2.1.Density Functional Theory (DFT)

For the longest time, experiments have been the main source of information about materials' properties. Understanding and characterizing materials through synthesis and testing in laboratories, has been the route availably taken even though it was occasionally troublesome. Therefore, researchers have always been trying to develop

theoretical methods that would allow them to predict the material's properties through fundamental laws of quantum mechanics.

In the domain of materials, knowledge of their electronic structure and thermodynamics is a key to unlocking their mysteries, allowing us to better understand their properties and create new functional materials. Because of the many-body issue, solving for a many-electron system is not as simple as solving a one-electron system. Thus, utilizing a full quantum mechanical calculation to model materials with many electrons and determine their electronic structure would need large memory and a long time to compute. As a result, for a material's computation to be both efficient and accurate, a type of mathematical approximation would be required.

For that reason, when stronger hybrid functionals with more refined exchange correlations models were being developed, especially after the 1990s, the successful Density Functional Theory (DFT) was seen as a breakthrough in the materials world. Today, modeling materials and predicting their properties have become more feasible and carried out routinely due to the great progress seen in electronic theory coupled with improvements on the computing side [7,12]. Many of the materials research that is seen today have utilized this computationally supported quantum mechanical model to predict and design novel materials under various conditions, as well as examine uncomprehended materials in depth by predicting their ground state energy and thus resolving their thermodynamics [28]. Experimental fields have been transformed by the ability to predict structure-property links. These advances in DFT have made it a vital tool that is used in different fields like solid-state physics, chemistry, material science, and many more [7,12].

The ultimate goal to generate information about a material is to acquire the ground state energy which is very challenging since it requires solving a complex quantum mechanical equation that accounts for individual electrons. This is where Density Functional Theory (DFT) offers a pleasant way around the many-body theory because it expresses the ground state energy of a uniform electron gas using a functional of the density F[n] [10]. A depiction of an electron gas density $n(r)$ is helpful since it facilitates an easier approximation solution due to the fact that it stays a three-

dimensional quantity portrayed as a field regardless of how many electrons are involved [10, 11].

Density Functional Theory (DFT) has gone through multiple stages of development from its early beginnings with the Thomas Fermi Method until the introduction of Kohn-Sham equations that brought it to where it is today [9, 13]. The latter has incorporated the variable function $n(r)$ into the ground state energy variational principal that is used in modern ground state energy in external potential calculations [10].

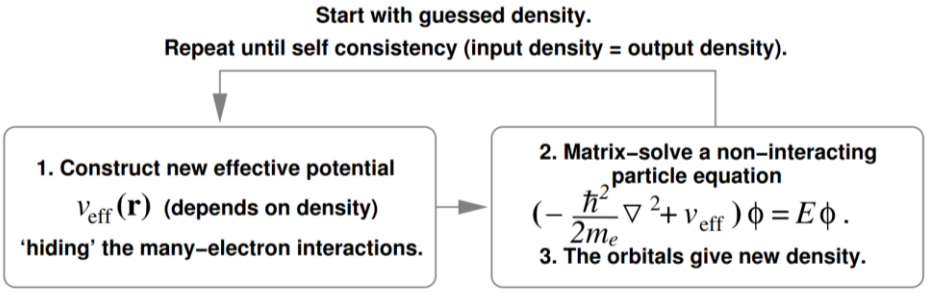

Figure [4]: A summary of the Kohn-Sham electron density minimization using a self-consistent solution [11].

Kohn-Sham equations also solve the electronic energy in a system, where the electron-electron interaction is ignored, by using a single particle orbital representation Ψ_i resulting in Kohn-Sham orbital energies ϵ_i [13]. The electron-electron interaction is then corrected through the single-particle potential by utilizing an exchange-correlation potential denoted as Vxc. This term approximation accounts for all the inconsequential many-body effects for the ground state [14]. The numerous approximation approaches employed in computing processes are distinguished by this exchange-correlation potential. Finally, this approach is summarized in Figure [4] where DFT starts with a predicted electron density and then attempts to minimize it to acquire a ground state energy by solving quantum mechanical calculations.

2.2. Exchange correlation XC and example functionals

The general ground-state calculations are carried out systematically through Kohn-Sham equations however, one example of a variational input of *ab initio* calculations is the exchange-correlation (XC) potential term approximation which is represented in the different functionals used for materials calculations. Over the past five decades, many functionals have emerged as universal functionals used for different materials

systems with electrons interacting via Coulomb potential [15]. These different functionals have also been studied to provide more customized calculations depending on the materials' specific intrinsic quantities. While there have been around 500 new functionals produced, some have been more widely incorporated in calculations due to their superior accuracy compared to the rest, such as BE from Perdew, Burke, and Ernzerhof [17,18], and the hybrid functionals B3LYP [19] and Heyd, Scuseria, and Ernzerhof's HSE06 which is used in this research [20,21] [15,16]. These many density functional approximations for XC are commonly organized into a "Jacob's ladder," with the top of the ladder corresponding to the most accurate functionals. The local density approximation is the earliest approximation for the XC potential found at the bottom of the ladder (LDA).

2.3. Generalized-Gradient Approximation (GGA)

This simple functional shows a dependence only on the particle density $n(r)$ at position r where it is evaluated [7]. The exchange-correlation hole is a crucial criterion that density functionals -including LDA- must satisfy. This exchange-correlation hole describes an area around a particle where it is less likely to locate an identical particle due to the Pauli exclusion principle. The energy is expressed by partitioning the exchange-correlation hole into an exchange and correlation components [22]. Thus, resulting in the following formula,

$$E_{XC} = E_X + E_C$$

However, this approximation has a great overbinding for exchange-correlation since it assumes that the electron density is constant all over. In order to account for this overbinding, a correction to LDA was applied in the form of a generalized gradient approximation (GGA) where Perdew showed a gradient correction to Ex in his following notation,

$$E_x(\rho) = \int e_X^{LDA}\,(\rho)\; f\; x(s)$$

Perdew and Wang in PW86 [23] showed that for the reduced density gadient ***s*** near atomic nuclei the electron densities are homogenous and towards the exponential tails they are inhomogeneous which is the opposite of how the gradient iself behaves [22]. Another type of GGA commonly used is Perdew, Becke, and Ernzerhof (PBE) functional [17], which is employed in this research, along with other functionals such as the Heyd, Scuseria, and Ernzerhof's (HSE06) hybrid functional to support any

overestimation made by GGA due to its overestimation of the electron delocalization caused by nonphysical electron self-interaction [7,17].

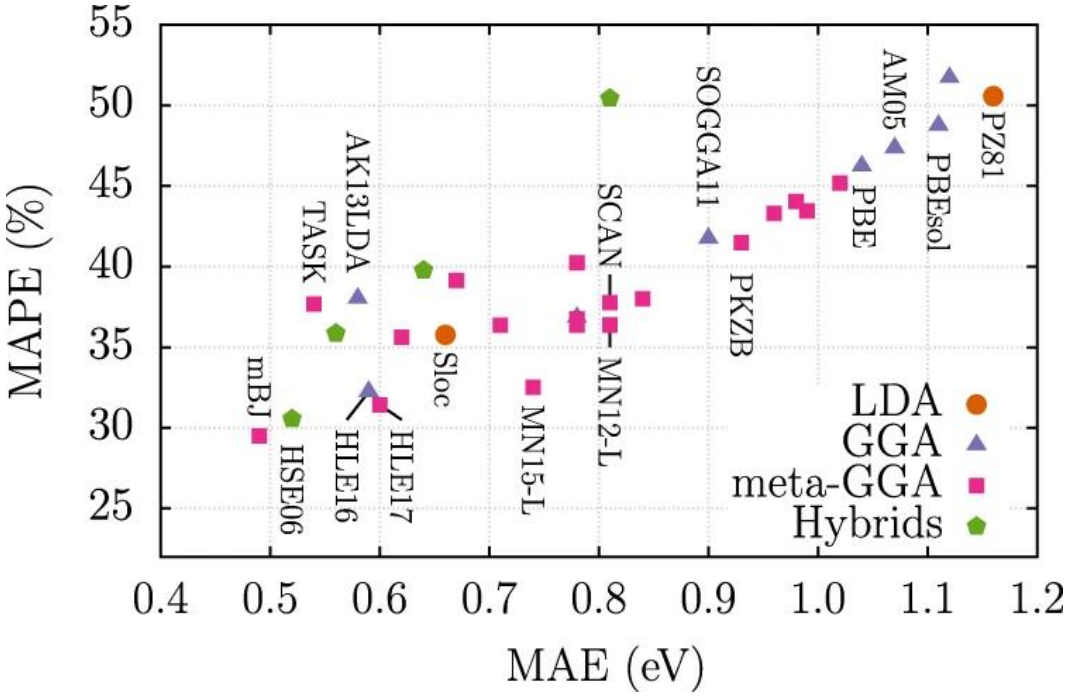

Figure [5]: A comparison between some functionals in terms of mean absolute error MAE and mean absolute percentage error MAPE [15]

2.4. Heyd–Scuseria–Ernzerhof (HSE) Hybrid Functional

Another functional which lies at a higher level on Jacoub's ladder compared to GGA due to its higher level of theory, yet lower than meta GGA which is considered superior, is the hybrid functional which HSE is a part of it. Such hybrid functionals account for a finer approximation for band gaps because they successfully contain the "non-dynamical correlations that delocalize the GGA exchange hole [20]". The exchange-correlation part of hybrid functionals is a blend of exact exchange in Hartree-Fock (HF) and LDA or GGA functionals [7,20]. This is due to the overestimation generated by HF of the bandgap and thus a combination of both HF and DFT functional could normally resolve this issue by meeting halfway. Gaussian-type orbitals are used in such hybrids along with periodic boundary conditions (PBC) [20]. Heyd, Scuseria, and Ernzerhof (HSE) employ a screening of the Coulombic potential of a shorter range where it splits the long- and short-ranged contributions, thus screening the Hartree-Fock HF term [7,20]. A combination of GGA and HSE06 hybrid functional was employed in this research.

3 Computational Methodology

The basis for most of the data generated was the crystal structure prediction of all the different pristine CSA compounds and their lithiated phases. This was done using an interplay of an evolutionary algorithm (EA) and Density Function Theory (DFT) calculations using USPEX and Vienna ab-initio simulation package (VASP) codes, respectively. A crystal structure is predicted solely knowing the chemical configuration with no need for experimental data since the evolutionary algorithm predicts different sets of generations of the crystal structure that is tweaked with fitness functions while looking for the structure with the lowest ground state energy with the help of DFT calculations that optimizes the geometry of each generation [24]. An initial population of 200 candidates was created for each structure calculation where this first generation was created with random crystal combinations by the EA and the structures geometrically optimized and relaxed using PBE-GGA (Perdew-Burke-Ernzerhof generalized gradient approximation) [18]. In order to predict a crystal structure that best embodies the global minimum of the system, different sets of qualities are sought out in each candidate, and as in nature, selection mechanisms to find candidates with the highest fitness are applied. This quality filtration system is realized using a set of fitness functions that go through each generation looking for certain properties and incorporated into the next generation. The different operations used in this research are fitness function, heredity function, mutation function (rotation), and a selection function. The fitness function selects the structures with the highest fit, or lowest energy, and inserts them into the next generation, while the others either combine two-parent candidates and produce an offspring with fused properties to have higher chances at finding the lowest energy

system or introduce mutations to the predicted structures that changes the orientation by rotating some functional groups [25,26]. The total number of generations selected for the CSA compounds was 30, where generation 0 was evolved from 200 candidates into the next generations with 20 candidates per generation. The volume size of each cell varied depending on the compound but ranged between 441 and 596 ($Å^3$). Furthermore, the accuracy of the basis set was controlled by the E_{cut} which is set to be 550 eV for all molecules. This process of using combined tools of USPEX and VASP to predict structures and relax them using DFT calculations is shown in Figure [6].

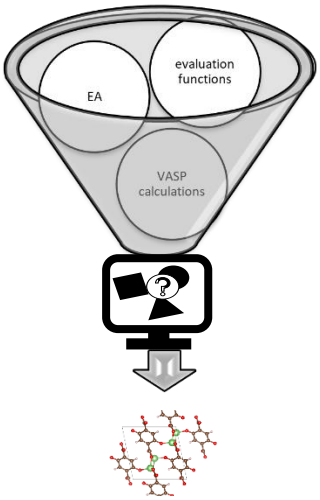

Figure [6]: An illustration depicting USPEX involving evolutionary algorithm with DFT calculations in VASP to compute crystal structures [28].

A GGA calculation was run for all compounds at different lithiation steps as a start point calculation with a (4x4x4) K-points and used to do a single gamma point combined calculation with GGA and geometrically optimized HSE06 hybrid functional. As a final structure prediction step, K-points were increased back to (4x4x4) and another combined GGA then an HSE06 calculation was run with no geometrical optimization in efforts to minimize computational time. This was done for all the different lithiation steps of p-PDSA, DM-PDSA, and DC-PDSA along with a Bader analysis, charge distribution analysis, and different data analysis for crystal structure like bond lengths.

4 Results

4.1 Crystal Structure

The ability to collect information on the crystal structure plays a vital role in understanding the structure's electrochemical qualities and redox reaction mechanism. This allows one to see where the lithiation occurs and how the structure changes through ion insertion. Moreover, it provides a better grasp of the system computationally where otherwise one has to do demanding experimental characterization. Depending on the type of material tested, it could be challenging to define crystallinity and form among other complexities. The crystal structures of Li_2-p-PDSA, Li_2-DM-PDSA, Li_2-DC-PDSA were predicted for their oxidized and reduced states through a genetic algorithm that is previously mentioned in the methodology section, coupled with a series of DFT calculations to generate the structure with the lowest energy or described as a relaxed ground-state structure. Figures [7] show the crystal structures generated and visualized through Vesta software where the atoms in red symbolize oxygen, yellow for sulfur, green for Lithium, blue for nitrogen, and the carbons in brown.

p-PDSA Li_0, p-PDSA Li_1, p-PDSA Li_3

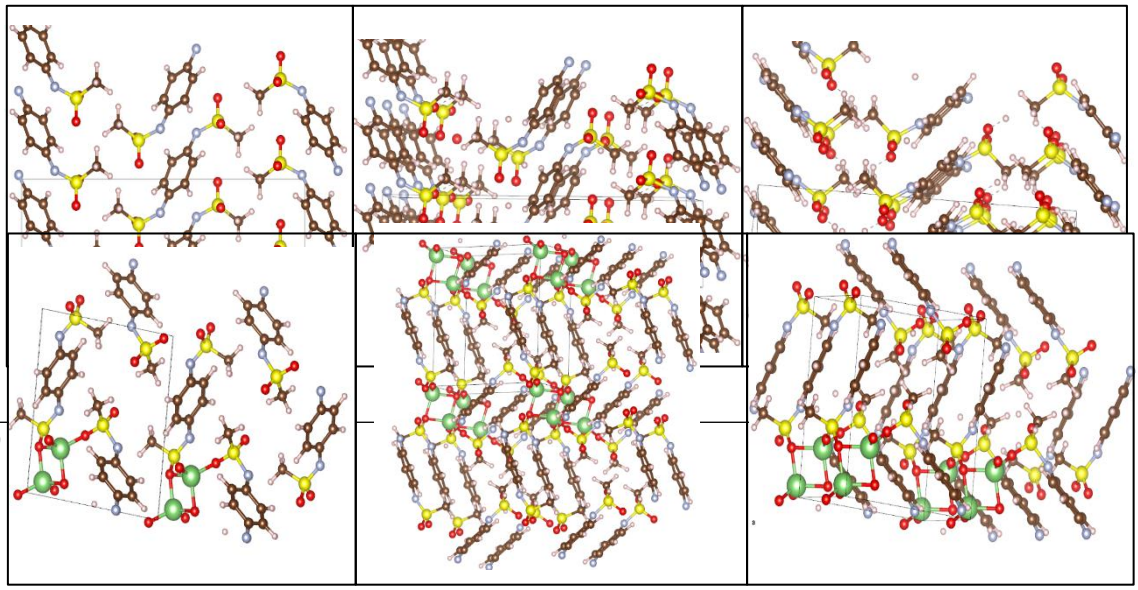

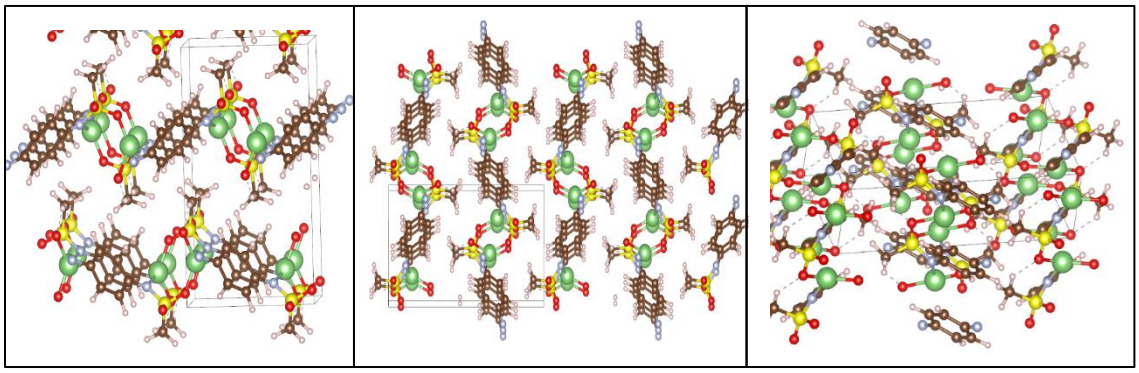

Figure [7]: The crystal structure generated using USPEX for p-PDSA during the first and second lithiation.

For the crystal structure of the pristine p-PDSA, it is visible how the nitrogen atoms are bonded to the sulfonyl groups in a trans arrangement. It is interestingly noted that after the first lithiation of this molecule, the cations approach the sulfonyl group bonding with the oxygens. Moreover, the structure seems to have a middle salt layer but with a few extra oxidized p_PDSA molecules bridging between the other layers. After the final lithiation where a total of two lithiums are inserted, the cell seems to become non-planar where the nitrogen is now bonded to the lithium along with two oxygens resulting in a mixture with two different configurations

DM-PDSA Li_0 , DM-PDSA Li_1, DM-PDSA Li_2

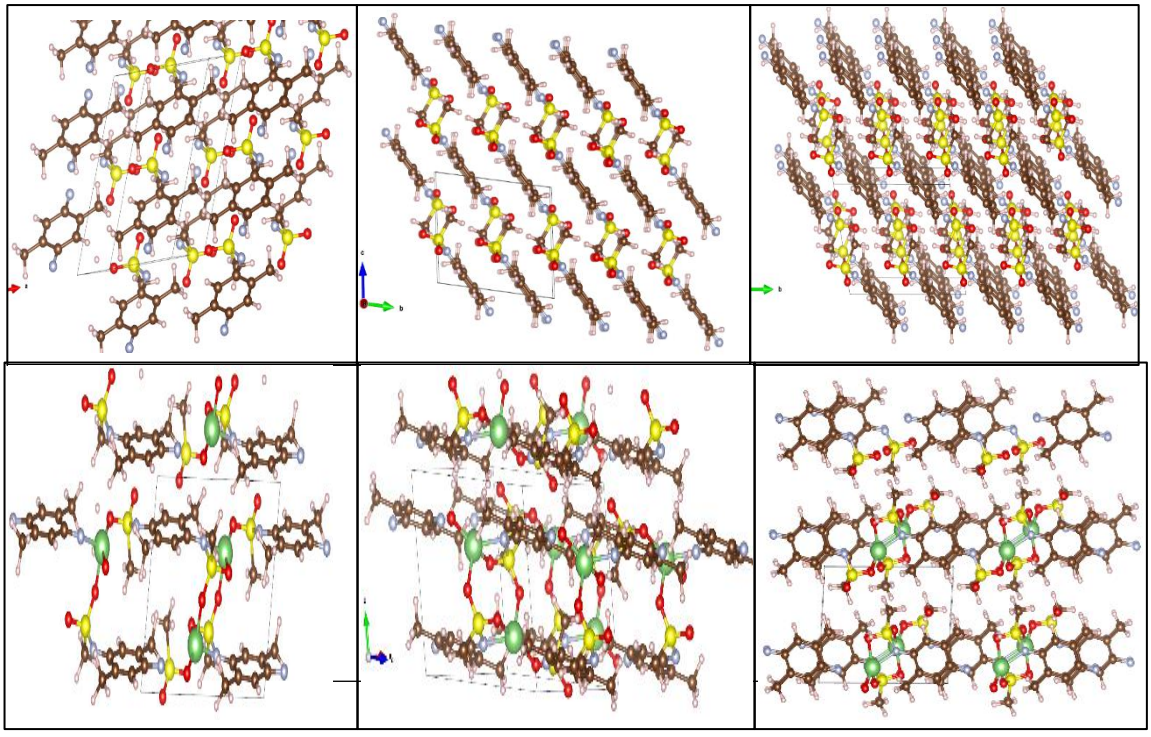

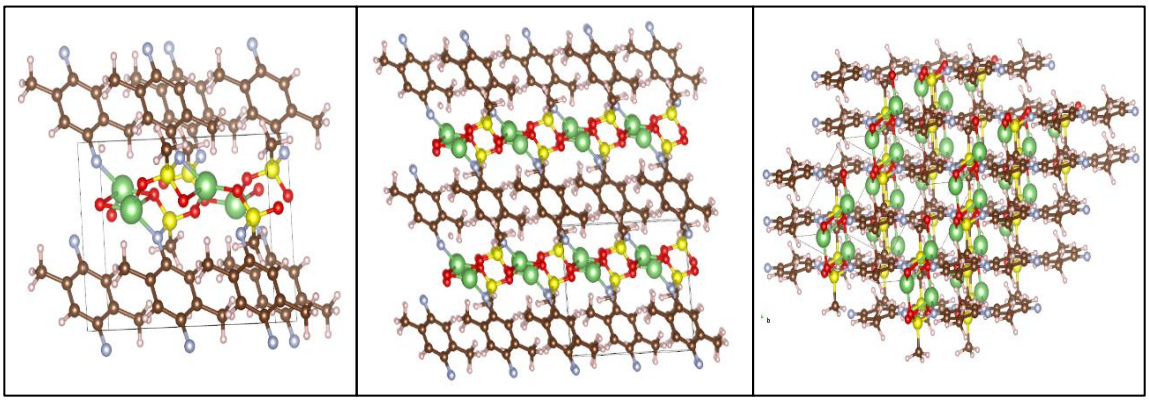

Figure [8]: The crystal structure generated using USPEX for DM-PDSA during the first and second lithiation.

As for the DM-PDSA molecule, the nitrogen seems to show a more prominent contribution to the lithium-ion from the first lithiation where it connects to it along with three other oxygens from different sulfonyl groups. After the second addition of the lithium-ion, a layer consisting of the lithium ions and sulfonyl groups arises in the middle, with benzene rings' part appearing to be planar.

DC-PDSA

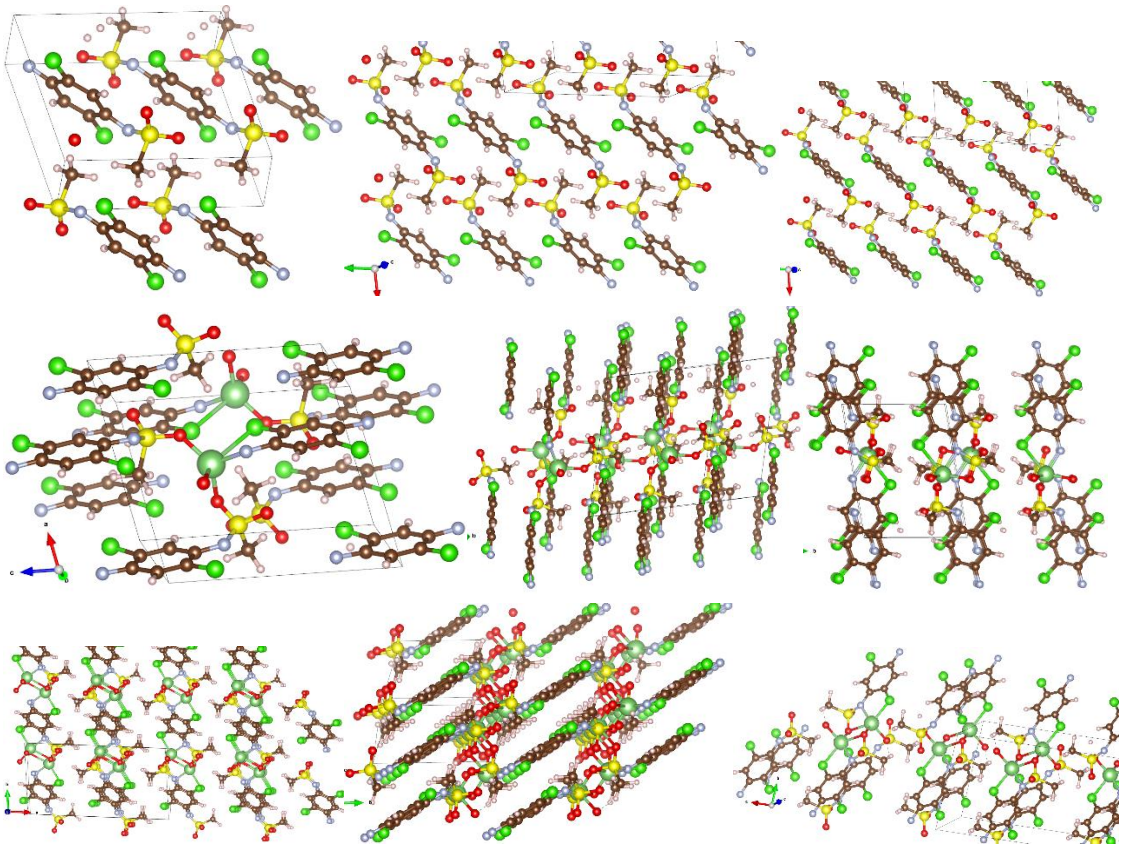

Figure [7]: The crystal structure generated using USPEX for DC-PDSA during the first and second lithiation.

The DC-PDSA molecule exhibits an organized system where the nitrogen and chlorides contribute to the lithium-ion coordination along with the oxygens from the sulfonyl groups after the first and second lithiation. The rings also appear to be in the same trans configuration consistently along with the cell. The space group and lattice parameters of the different crystal structures during different lithiation steps have shown to be P1.

	A (Å)	B (Å)	C (Å)	P-PDSA			DM-PDSA			DC-PDSA		
	A (°)	β (°)	γ (°)									
LI_0				4.65308	4.79740	18.48952	7.46659	10.40698	7.40086	7.52491	10.43738	7.38821
				89.9998	90.0001	85.4687	90.0000	90.0000	90.0000	109.7956	94.3834	97.1984
LI_1				9.23740	5.11608	10.37413	7.93369	7.66627	9.86567	8.18714	8.15816	10.18319
				94.8881	93.1955	95.8021	99.0743	86.0173	94.6785	103.3243	77.1470	111.3658
LI_2				14.37421	7.94282	4.52524	10.54889	8.19006	7.18560	15.34078	8.08809	4.55526
				84.7196	90.0400	89.8965	78.6913	109.6310	90.2131	73.4849	93.5821	95.1186

Table [2]: Cell unit information showing the lattice parameters of the studied CSA compounds throught out lithiation.

Bond Lengths

p-PDSA	*Li_0 (Å)*	*Li_1 (Å)*	*Li_2 (Å)*
C=C	1.35	1.38	1.39
C-C	1.44	1.40	1.41
N-C	1.31	1.29, 1.38	1.39
N-S	1.65	1.66, 1.51	1.55
N-Li	N/A	N/A	1.96
Li-O	N/A	1.78, 1.91, 1.98, 2.00	2.01, 1.87
S-O, S-CH3	1.43, 1.43, 1.76	1.42, 1.43, 1.74 1.43, 1.48, 1.76	1.4, 1.4, 1.75

Table [3]: The bond length of some bonds for p-PDSA noted for the pristine form and after lithiation.

We see an increase in C-N bond length after lithiation which means the Li-ion is destabilizing the C-N bonds in these systems. On the other hand, data shown in table 3 presents a decrease in the S-N bond length which explains the stabilizing effect of lithiation for the S-N bonds, which agrees with the literature. Moreover, the single and double C-C bonds seem to come to similar bond lengths which suggests the aromaticity of benzene in mentioned systems that is more prominent after the Lithium-ion insertion.

In the Li_1 structure of p-PDSA, there seem to be mixed structures as seen in the bond lengths table where the C-N and S-N bonds seem to change between main layers' structure or ones found in between layers. These two structures have either a shorter C-N double bond (1.29Å) and a longer S-N bond (1.66Å) compared to Li_0 and a longer C-N single bond (1.38Å) and a shorter S-N (1.51Å) bond compared to the delithiated phase. According to the CSA family paper, the compound p-PDSA is the only one that provides a hysteresis from the first cycle due to it being a polymorph where the redox reaction mechanism involves a radical that has a C=N double bond and a C-N single with a Li bonded to it. Our results indicate that the mixture could happen in a similar way where two different structures are existing in the same cell where one shows a quinoneimine appearance and the other a phenylenediamine.

DM-PDSA	Li_0	Li_1	Li_2
C=C	1.45	1.43	1.40
C-N	1.29	1.34, 1.35	1.39
S-N	1.63	1.58	1.54
N-Li	N/A	2.1	1.97
S-O, S-CH3	(1.43,1.43), 1.74	(1.44,1.45),1.74/one1.76	(1.46,1.46), 1.76
CH3-ring	1.48,1.48	1.48, 1.49	1.50
O-Li	N/A	1.95,1.95,2.01	1.87,1.88,2.5

Table [3]: The bond length of some bonds for DM-PDSA noted for the pristine form and after lithiation.

DC-PDSA	Li_0	Li_1	Li_2
C=C	1.45	1.44	1.42
C-N	1.29	1.33	1.38
S-N	1.64	1.58/1.59	1.54
Li-N	N/A	2.04	2.00
Li-O	N/A	1.86, 1.97, 2.09	1.86, 1.98, 2.53
Li-Cl	N/A	2.84	2.47
S-O, S-CH3	(1.43,1.43), 1.74	(1.44,1.45),1.74/one1.75	(1.45, 1.46), 1.76
Cl-ring	1.69	1.71	

Table [3]: The bond length (Å) of some bonds for DC-PDSA noted for the pristine form and after lithiation.

For the DM-PDSA and DC-PDSA molecules, a similar pattern as p-PDSA is observed where the C-N bond is elongated after lithiation while the S-N bond is shortened and stabilized. As for DM-PDSA, the CH3 group that is attached to the ring seems to have an increase in bond length between it and the ring after introducing the two electrons to the system. While DC-PDSA shows an increase in the bond length as well of the C-Cl bond after lithiation where the Cl atoms also bond to the incoming lithium ions. Overall, the lithiation process seems to increase the aromaticity of the three systems which also concur with the CSA family paper published by Nature Materials [5].

4.2 Potential Energy / Voltage Profile

With the information about the ground state of the different structures in hand, a thermodynamical evaluation of the system is obtained. Some pieces of information one can calculate, are the voltage profile and the potentials change after each lithiation

step which shows its effect on the system. Table 4 shows the potential of the three CSA compounds calculated for the single electron step as well as the two electron-step, where the latter is how the redox reaction is executed in these systems. The tables also show the difference in voltage generation between the two different functionals discussed previously in the theory section, GGA, and HSE06. A trend is observed where using GGA results in a lower value for the voltages for p-PDSA and DM-PDSA and using HSE06 yields a higher voltage which is closer to the experimental values. However, this trend seems to be the opposite for the DC-PDSA system.

p-PDSA (GGA)			
	Energy	1-step Potential (V)	2-step Potential (V)
Li0	-319.58309311		2.94 V (exp = 2.95 V)
Li1	-329.53069216	3.08	
Li2	-338.94488731	2.81	

p-PDSA (HSE06)			
	Energy	1-step Potential (V)	2-step Potential (V)
Li0	-379.67766112	-	3.31 V (exp = 3.15 V) Solid phase
Li1	-391.54338012	3.96 V	
Li2	-400.78467324	2.65 V	

Table [4]: The energy results and calculated voltage for p-PDSA for single step and two-step reactions using GGA and HSE06.

For the p-PDSA structure, the overall voltage is shown to be at 2.94 V while the generated using HSE06 is at 3.31 V which is closer to the experimental value of 3.15 V for the structure in the solid phase. As for DM-PDSA, the two-electron redox reaction is calculated to be at 3.14 V where the experimental value matches to be 3.05 V within a margin of ~ ±0.1V. The potential generated with GGA shows an underestimate with a value of 2.89 V, where it is coincidently close to the theoretical potential calculated

in the original paper where they have modeled the compounds in solution with a value of 2.76 V, therefore yielding slightly different results, which they discussed the effect of phase-type in exhibiting different electrochemical properties. Finally, the compound DC-PDSA shows a voltage of 2.90 V using HSE06 functional and 3.37 V with GGA where they both compare with the experimental at a value of 3.35 V.

DM-PDSA (GGA)			
	Energy	1-step Potential (V)	2-step Potential (V)
Li0	-387.22147213		2.89 V (exp = 2.77 V) liquid phase (Theor = 2.76 V)
Li1	-396.85114528	2.92	
Li2	-406.37029052	2.86	
DM-PDSA (HSE06)			
	Energy	1-step Potential (V)	2-step Potential (V)
Li0	-459.93309307		3.14 V (exp = 3.05 V) solid phase
Li1	-470.08946528	3.11	
Li2	-480.35877203	3.16	

Table [5]: The energy results and calculated voltage for p-PDSA for single step and two-step reactions using GGA and HSE06.

DC-PDSA (GGA)			
	Energy	1-step Potential (V)	2-step Potential (V)
Li0	-313.71204073		3.37 V (exp = 3.35 V) Solid phase
Li1	-323.67232064	3.08	
Li2	-333.84632582	3.19	
DC-PDSA (HSE06)			
	Energy	1-step Potential (V)	2-step Potential (V)
Li0	-377.40137670		

Li1	-388.01713316	3.34	
Li2	-396.87884227	2.46	2.90 V (exp = 3.35 V) Solid phase

Table [6]: The energy results and calculated voltage for DC-PDSA for single step and two-step reactions using GGA and HSE06.

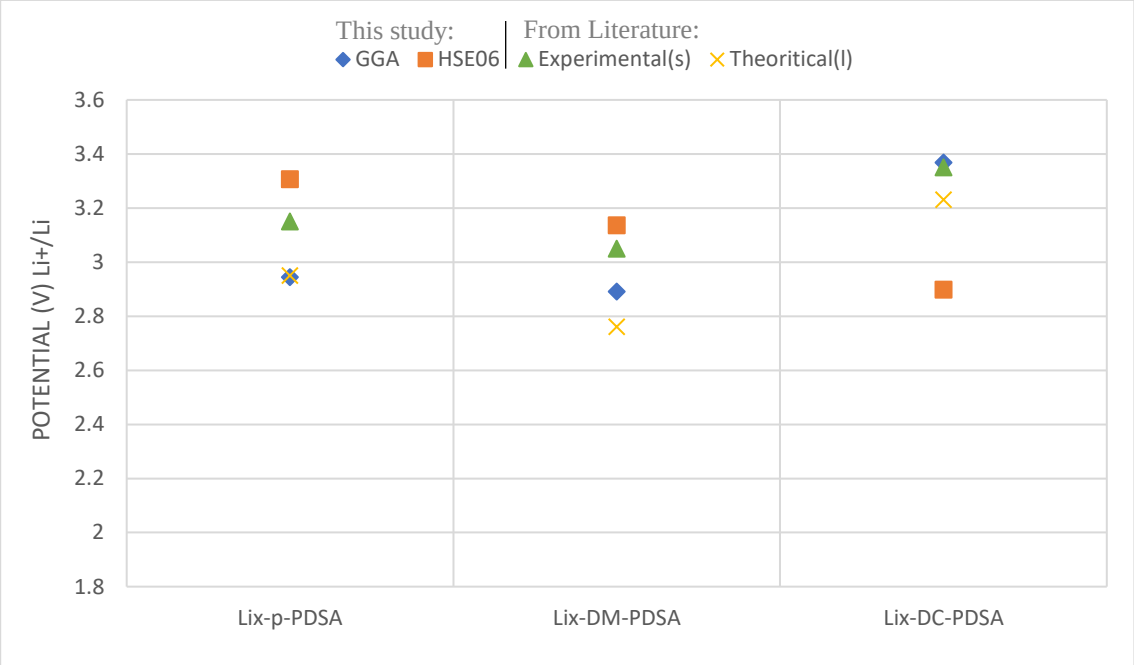

Figure [8]: A comparison of the potential in V for the different CSA compounds between the reuslts using GGA, HSE06, literature's experimental in solid and theoritical in liquid.

Figure 8 shows a comparison for the three compounds between the two-electron reaction potential generated by this research using GGA and HSE06, as well as the experimental (in solid) and theoretical (in solution) results recorded in the original paper. As seen from the figure, the SHE06 functional seems to provide a close result compared with the experimental values for the compounds p-PDSA and DM-PDSA while GGA performs better for DC-PDSA. Another observation is that there seems to be a decrease in the potential when calculating for compounds in solution compared to the solid phase and that is why the underestimate usually seen in GGA functional shows closer values compared to theoretical results for the liquid phase.

4.3 Electronic Structure

The density of States/ Charge distribution

p-PDSA

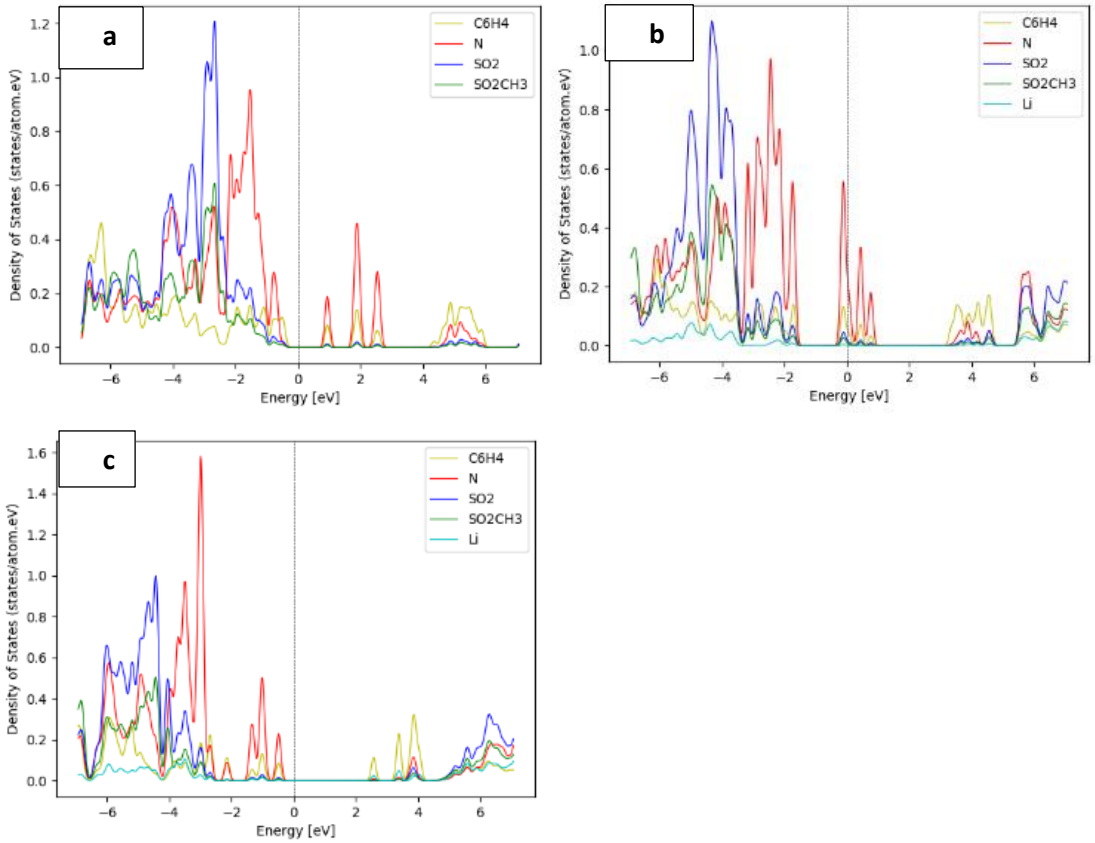

Figure [9]: The density of states plotted for DOS for p-PDSA in delithiated state in (a) and first lithiation (b) second lithiation (c).

The electronic structure was calculated from the DOSCAR generated by the DFT calculations in VASP which provides vital information about the redox reaction during the different lithiation steps and displays its effect on the electronic structure. In figure 9, the density of states (DOS) for p-PDSA appears to have empty atomic orbitals that are ready to be populated which is what happens during the insertion of the first lithium to the system where the orbitals are partially filled. Those partially filled orbitals in the Li_1 structure have higher states from nitrogen then comes states for the ring and then the sulfonyl SO_2 group. For that reason, the atomic orbitals that get filled after the final lithiation, which rounds up to a two-electron reaction, are mainly the nitrogen group with its three peaks along with the ring C6H4 and the SO2 groups which are all now fully occupied with an increased fermi gap.

The previous information from the density of states is then supported by a charge density study of the system where figure 10 shows how the charge is distributed along

with the system in its different lithiated steps. The charge is observed to be more delocalized around the aromatic ring after the second lithium insertion along with a charge distribution around the nitrogen atom that spread towards the sulfonamide group upon lithiation. It is also noted that for Li_1-p-PDSA, where there seems to exist a mixture of structures, the structures with a lone pair on the nitrogen groups show a charge delocalization around the sulfonamide group, while the middle structures where quinonimine like composition seems to show no charge distribution.

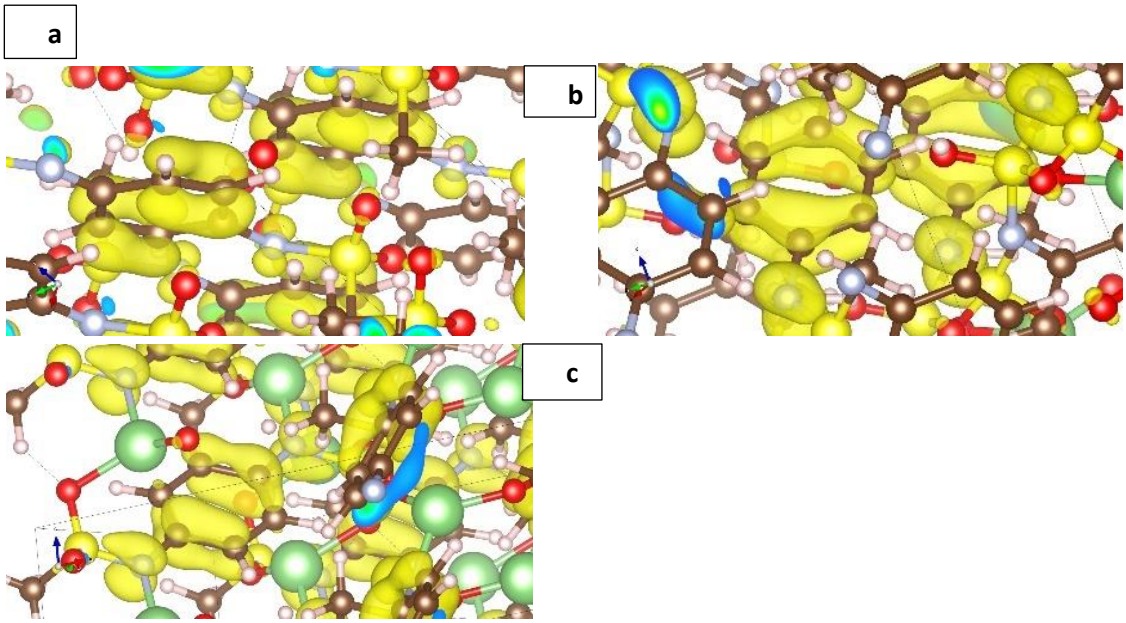

Figure [10]: The charge density distribution evolving from the pristine form in (a) to 1st lithium addition in (b) and second in (c).

DM-PDSA

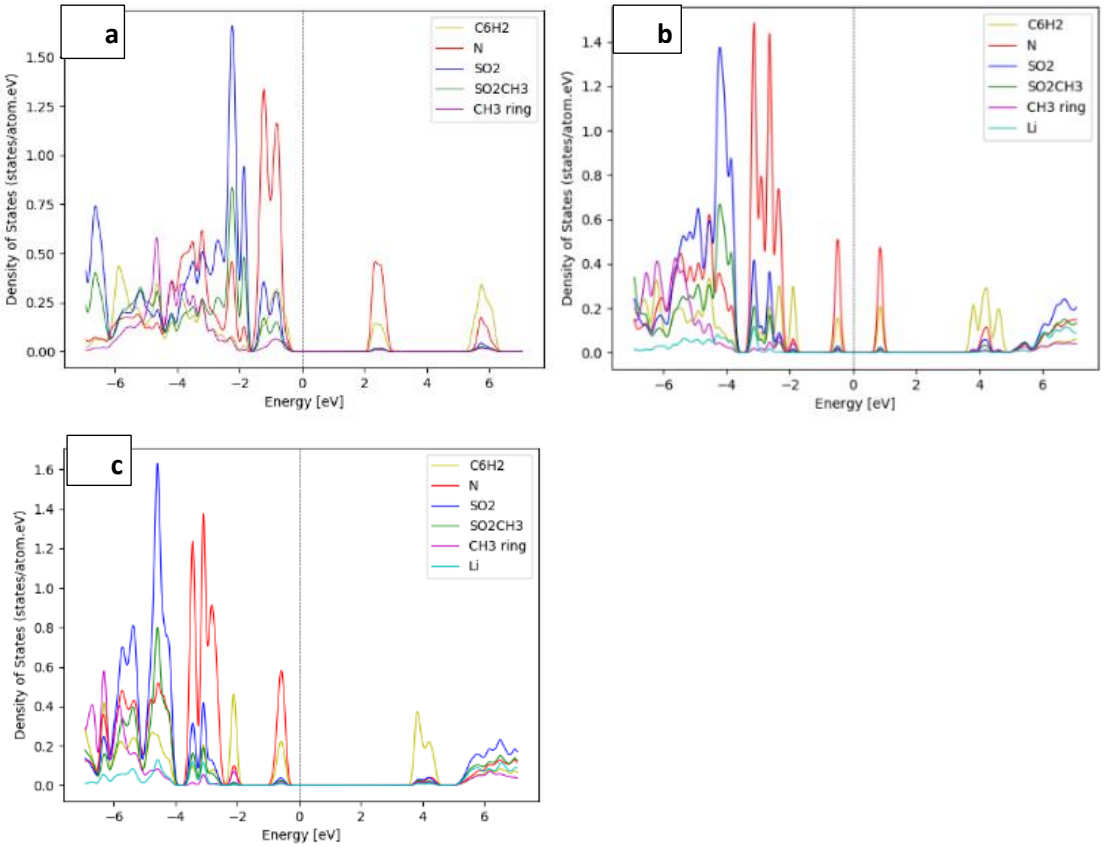

Figure [11]: The density of states plotted for DOS for DM-PDSA in delithiated state in (a) and first lithiation (b) second lithiation (c).

The DOS for DM-PDSA shows empty atomic orbitals that the nitrogen contributes along with the ring and SO2 groups where it supports the fact that the sulfonamide group is a strong electron-withdrawing group. This is visible after lithiation where the nitrogen mainly, but the sulfonamide orbital gets filled with empty orbitals for the ring further away. Figure 12 showing the charge distribution also confirms that the sulfonamide's electron-withdrawing effect delocalizes the charge along with the sulfonamide group and specifically the nitrogen. Moreover, the methyl group connected to the ring also seems to play a role in the charge density for the pristine structure where some charge is localized near its hydrogen. However, this seems to disappear after the first and second lithiation steps where a charge delocalization around the ring shows an increase in its aromaticity in the reduced state.

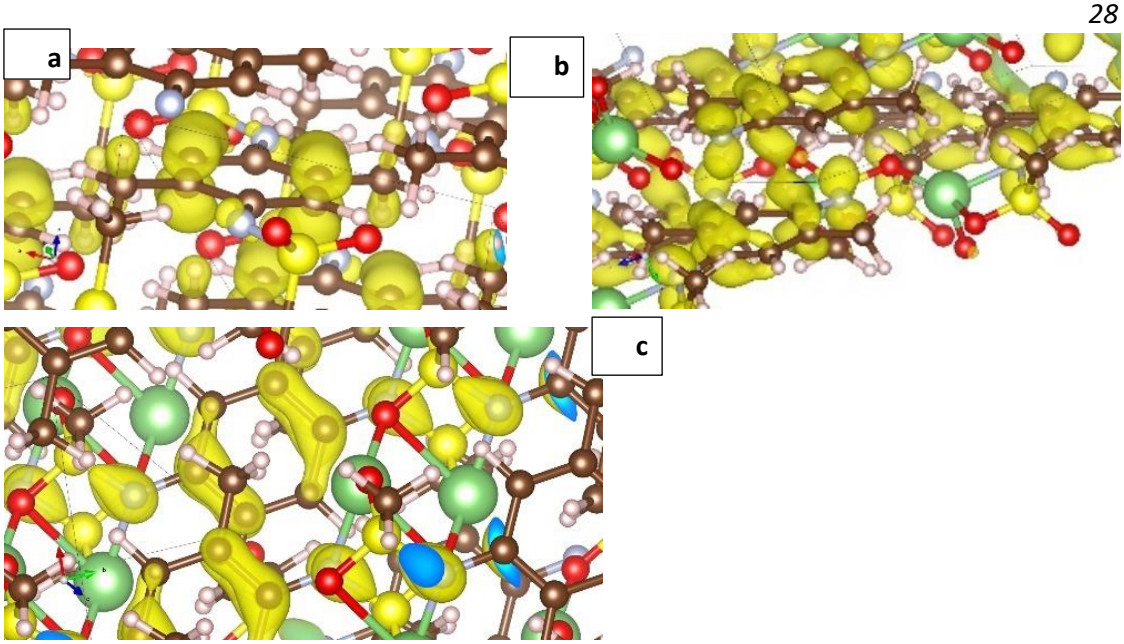

Figure [12]: The charge density distribution for DM-PDSA evolving from the pristine form in (a) to 1st lithium addition in (b) and second in (c).

DC-PDSA

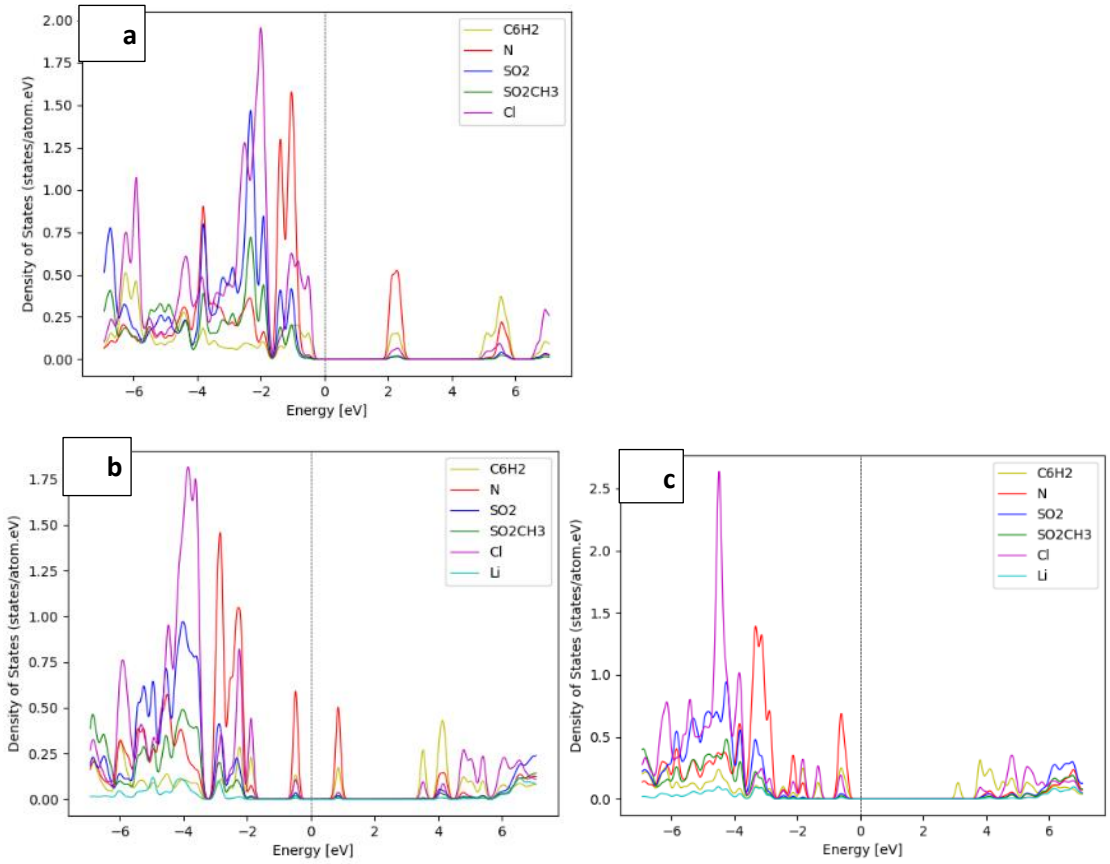

Figure [13]: The density of states plotted for DOS for DC-PDSA in delithiated state in (a) and first lithiation (b) second lithiation (c).

The DC-PDSA compound seems to follow similar trends as the other molecules in terms of electronic structure, however, an additional contribution to the empty atomic states near the Fermi level comes from the chloride atoms. This is then fully populated after the second lithiation where the other nitrogen and sulfonyl groups states are occupied. In the charge density figure 14, one observes a charge around the chlorides in the pristine form and around the ring but with the insertion of lithium, a shift in the electron density is seen. The chlorine loses its charge density while the nitrogen gains some of which is delocalized around the sulfonamide group. Also, the ring shows a greater charge delocalization than before proving again in aromaticity discussed in bond lengths.

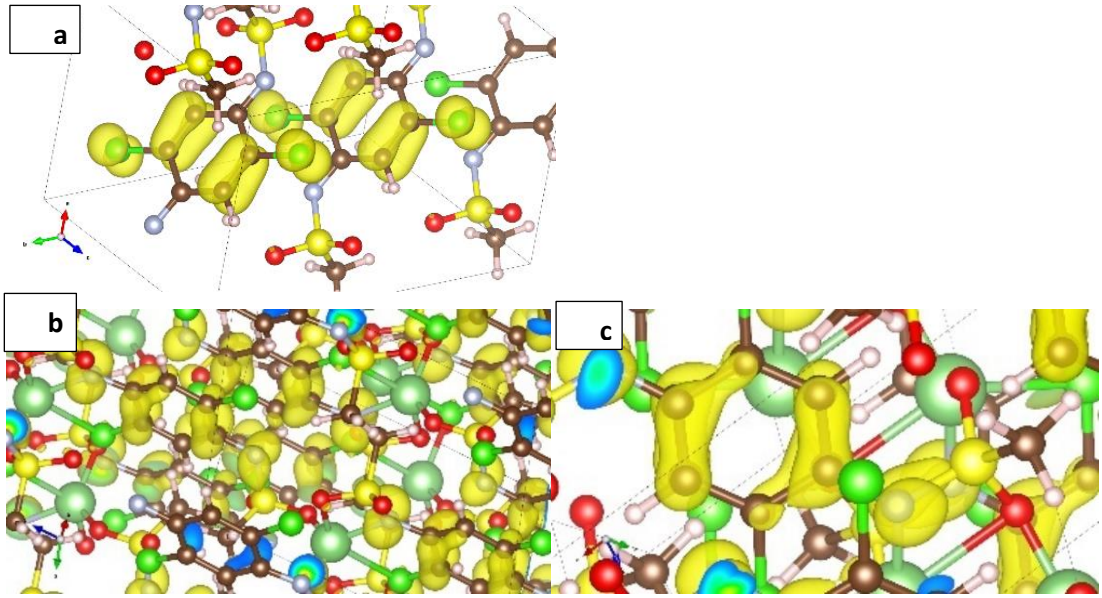

Figure [14]: The charge density distribution for DC-PDSA evolving from the pristine form in (a) to 1st lithium addition in (b) and second in (c).

4.4 Bader Analysis

A Bader charge analysis was carried out which calculated the net charge that corresponds to every single atom using a zero-flux surface method to differentiate atoms with charge value from spaces between atoms that have a minimum charge density perpendicular to the surface [27]. Figure 15 shows the net charge per atom for p-PDSA where the charge delocalizes along the organic molecule with an increase in aromaticity where the highest charge is found around the ring. The sulfonyl group

comes in second place where it also observes a charge localization around it. It is interesting to conclude previous propositions with the single electron step Bader analysis where one sees a drop in the SO2 group after the first lithium insertion. This could support the crystal structure prediction where those ionized sulfonyl groups have a lower electron charge due to the oxygens being involved with the lithium ion.

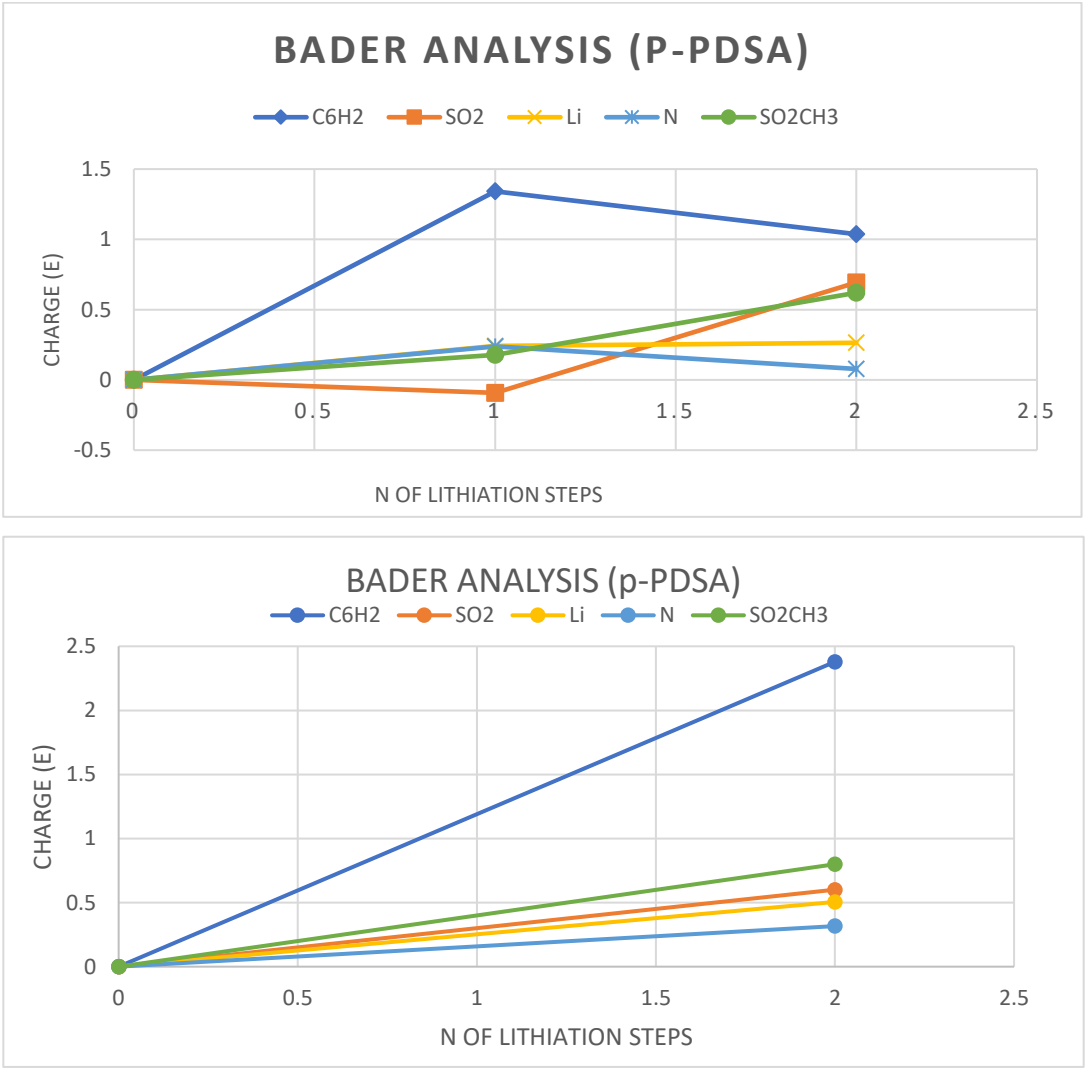

Figure [15]: A Bader charge analysis with single step (top) and two step redox reaction (bottom) for p-PDSA.

As for DM-PDSA, the two-electron step shows a greater net charge for the SO2CH3 groups where a dip in the nitrogen charge after bonding to the lithium ions during reduction leaves greater net charge for atoms/groups such as lithium, methyl groups connected to the ring, and the aromatic ring.

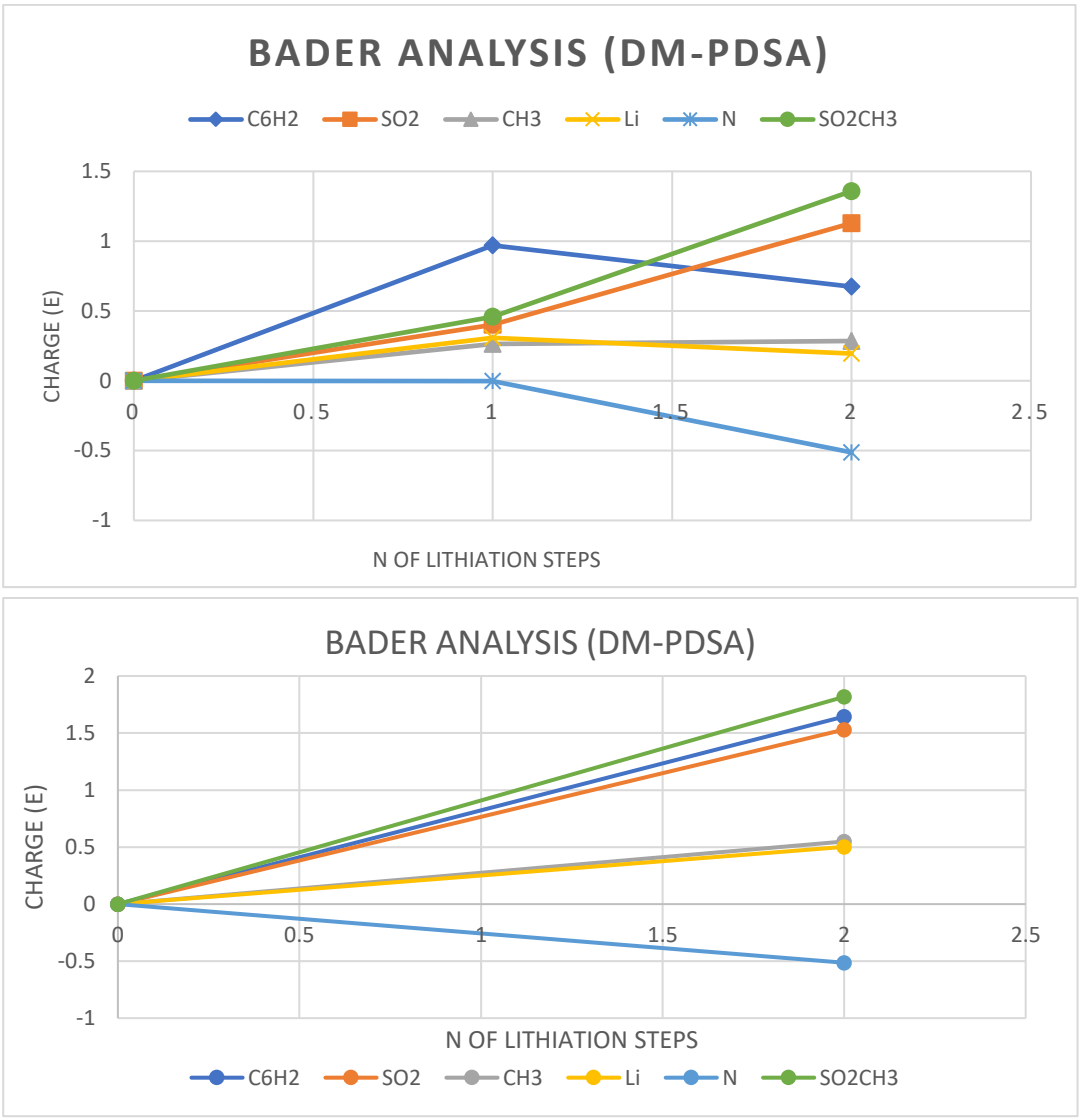

Figure [16]: A Bader charge analysis with single step (top) and two step redox reaction (bottom) for DM-PDSA.

The Bader analysis for DC-PDSA shows that after the second lithiation, the charge on the nitrogen atom decreases since it is now fully occupied in agreement with the density of states figure. It also further supports other information from DOS where a charge delocalization is surrounding the ring and then the sulfonyl group has charge after lithiation. This is due to the effect of the sulfonamide group mitigating charge on all sulfonamide groups and partially to the ring thus stabilizing it.

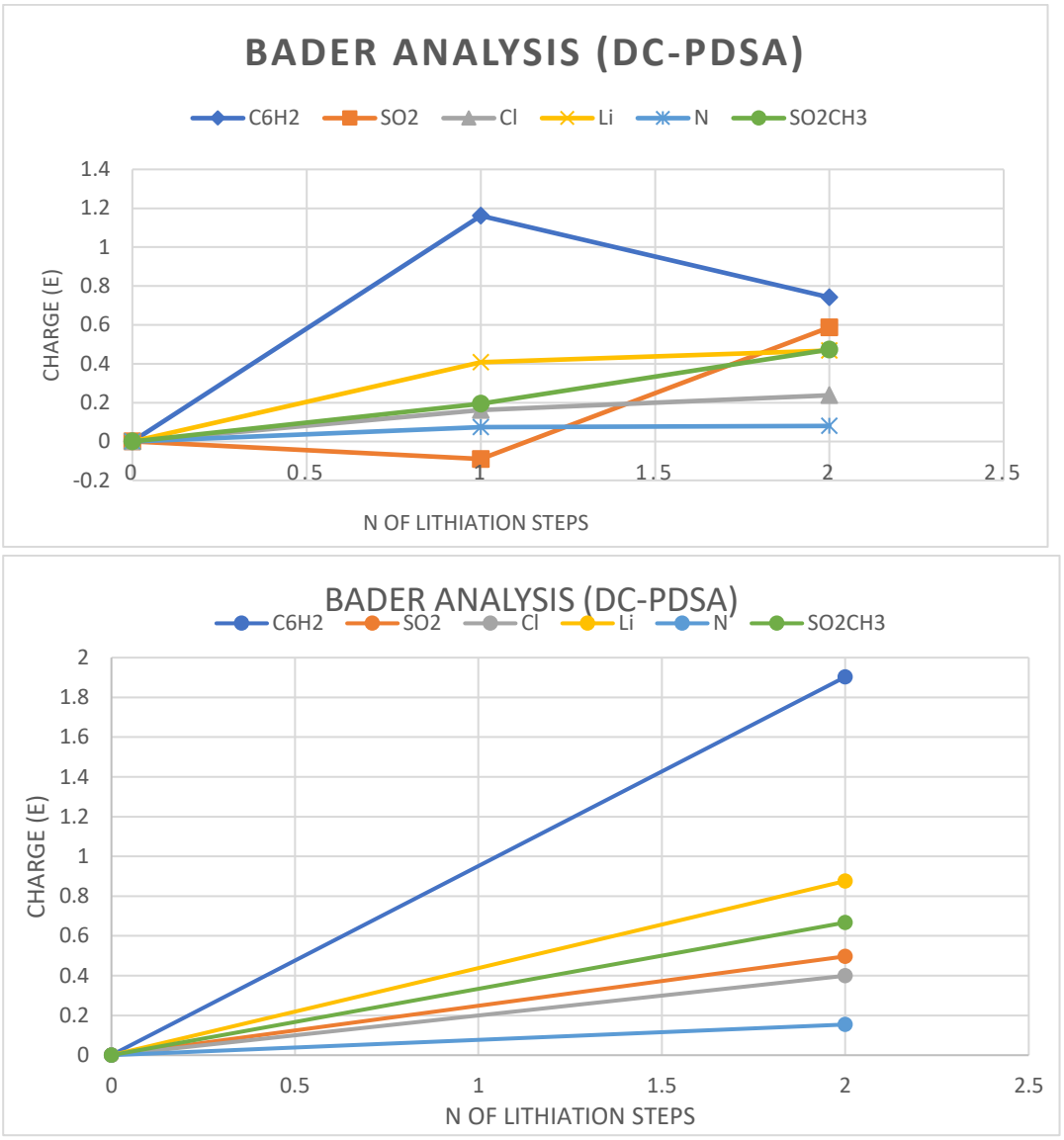

Figure [17]: A Bader charge analysis with single step (top) and two step redox reaction (bottom) for DC-PDSA.

4.5 Previous Results/other quinone systems

Previous research on the Lithium (2,5-dilithium-oxy)-terephthalate structure during multiple lithiation steps was done computationally using the same geometrically optimized HSE06 procedure which resulted in a good understanding of the system structurally and thermodynamically. This quinone carboxylate system seen in figure 18 originates from the same tree of lithium-ion organic cathode materials including the CSA family. The voltage calculation for the system between Li_2-p-DHT/ Li_4-p-DHT was 2.6 V where it compares to experimental results of 2.7 V [28].

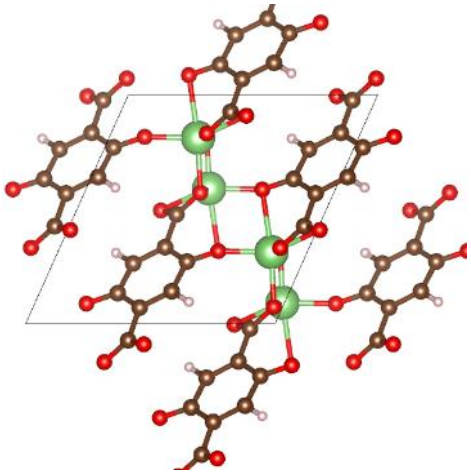

Figure [18]: A crystal structure predicted using USPEX/VASP for Li2-p-DHT [28].

A DOS and a Bader analysis in the second lithiation step going to Li_4-p-DHT in figure 19 shows how the system moves forward from charge localization around the ring's oxygen to a higher total charge of the carboxylate group COO^-. This is explained by the charge distribution and Bader analysis where the aromatic ring is then enriched by a charge due to the electron donation effect coming from the oxygens first then mainly the carboxylates. The main reason these quinone systems result in comparatively decent redox potential is because of the ability to stabilize the aromatic system. This is partially achieved due to the +I inductive effect posed by O^- and COO^- where they mitigate the charge to the ring thus enriching it [29].

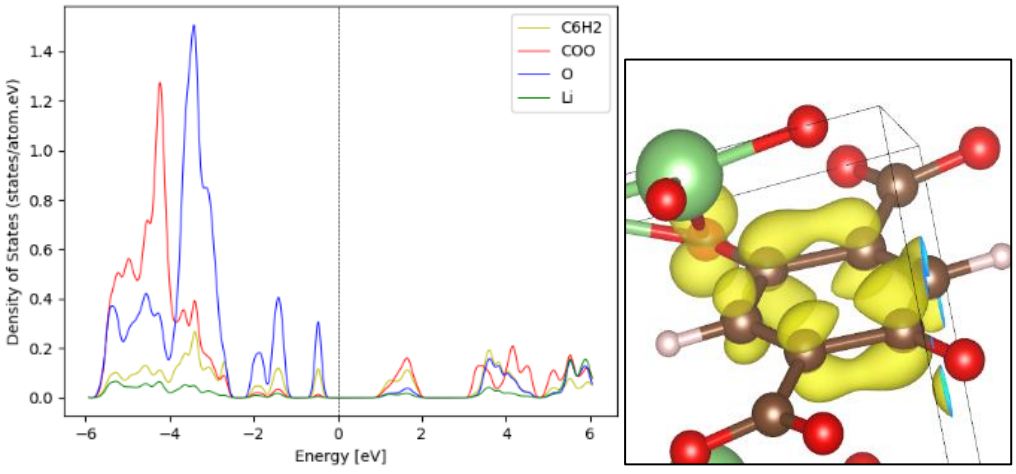

Figure [19]: A density of states (left) during the second lithiation of Li4-p-DHT [28].

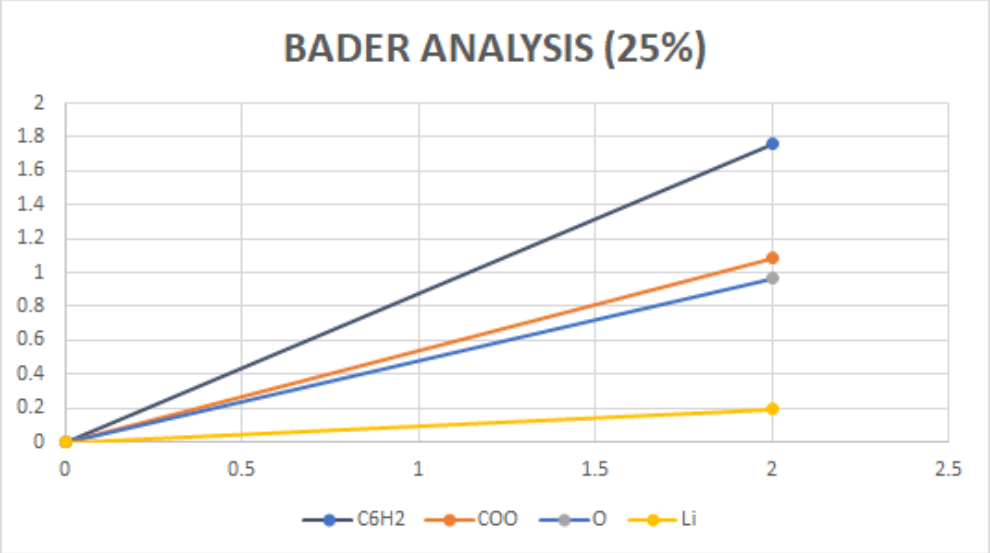

Figure [20]: A Bader charge analysis for Lix-p-DHT using a 25% exchange correlation and geometric optimization for HSE06. [28]

5 Conclusion

Organic electrode materials (OEMs) have been studied lately as an alternative way from inorganic materials to store energy due to many environmental and financial benefits. However, finding an organic cathode material with a redox potential powerful enough to compete with its inorganic counterparts has been quite challenging and scarce. The paper Wang et al. [5] put forth a state-of-the-art class of organic lithium-ion cathodes, conjugated sulfonamides, that posses' electrochemical properties almost matching some of the most iconic inorganic cathodes, while also being stable in ambient conditions. Three different compounds from the CSA family were studied in this thesis p-PDSA, DC-PDSA, and DC-PDSA during two lithiation steps where a genetic algorithm was employed using USPEX to predict the crystal structures along with VASP to conduct DFT calculation. Those crystal structure predictions allowed for the analysis of the electronic structure of the different systems which provided insight into the electrochemical mechanisms of such systems and some understanding of their voltage profile that was calculated to be between 2.9 and 3.3 V using HSE06 hybrid functional. Previous results from another quinone system with a carboxylate group provided a perception of the electrochemical tuning of these cathode systems whether they were quinones or quinonimines. Briefly, in order to increase the redox potential of the organic system, a sort of tuning of the p-electron density of the aromatic skeleton should take place. In the case of Lithium (2,5-dilithium-oxy)-terephthalate, the carboxylate group COO^- is reducing the charge to the ring and thus stabilizing it, although, the voltage produced by the introduction of two lithium ions are relatively low (2.6V) compared to the new CSA family which offers an improvement beyond the lithium-ion cathode materials with further tuning possibilities. In the case of the CSA compounds, the sulfonamide group plays a vital role in mitigating charge on all sulfonamide groups and partially to the ring and

increasing the aromaticity. The three different systems studied in this research are conjugated since the backbone has an overlap of p orbitals where the results show a charge delocalization which supports alternating single and double bonds, and thus conjugation. Having a sulfonamide group introduced to these organic electrode systems as an electron-withdrawing group (EWG) helps stabilize the system through delocalization of charge along the sulfonamide group thus minimizing a localization on the nitrogen as well as nucleophilicity as proposed in Wang et al. paper and shown in results. These properties aid the CSA family to have a reversible redox reaction with high energy densities which makes them promising high-performing organic cathode materials that push the frontiers of powerful organic cathodes.

Bibliography

1. Manthiram, A. A reflection on lithium-ion battery cathode chemistry. Nat Commun 11, 1550 (2020). https://doi.org/10.1038/s41467-020-15355-0
2. LITHIUM-ION BATTERIES." Nobel Prize, The Royal Swedish Academy of Sciences, 9 Oct. 2019, www.nobelprize.org/uploads/2019/10/advanced-chemistryprize2019.pdf[2] nobel prize: LITHIUM-ION BATTERIES." Nobel Prize, The Royal Swedish Academy of Sciences, 9 Oct. 2019, www.nobelprize.org/uploads/2019/10/advanced-chemistryprize2019.pdf.
3. La1kraychi, Alae Eddine, and lexandru Vlad. "Organic Batteries - the Route towards Sustainable Electrical Energy Storage Technologies." *Chimie Nouvelle*, Institut De La Matière Condensée Et Des Nanosciences (IMCN), Université Catholique De Louvain, Place L. Pasteur 1, 1348 Louvain-La-Neuve, Belgium, 2018, chimienouvelle.be/CN127/Article%20Lakraychi.pdf.
4. High-voltage positive electrode materials for lithium-ion batteries, Wangda Li,Bohang Song, and Arumugam Manthiram*Materials Science and Engineering Program andTexas Materials InstituteUniversity of Texas at Austin
5. Wang J, Lakraychi AE, Liu X, et al. Conjugated sulfonamides as a class of organic lithium-ion positive electrodes. *Nature materials*. 2021;2020;20:665-673.
6. Song, Z., & Zhou, H. (2013). Towards sustainable and versatile energy storage devices: An overview of organic electrode materials. Energy & Environmental Science, 6(8), 228-231. doi:10.1039/c3ee40709h
7. Heiska, J., Nisula, M., & Karppinen, M. (2019). Organic electrode materials with solid-state battery technology. Journal of Materials Chemistry A, 7(32), 18735-18758. doi:10.1039/c9ta04328d

8. Poizot P, Gaubicher J, Renault S, Dubois L, Liang Y, Yao Y. Opportunities and Challenges for Organic Electrodes in Electrochemical Energy Storage. Chemical reviews. 2020;120:6490-6557.
9. *N. H. March, Advan. Phys. 6, 1 (1957)*
10. Hohenberg P, Kohn W. 1964 Inhomogeneous electron gas. Phys. Rev. 136, B864–B871. (doi:10.1103/PhysRev.136.B864)
11. Armiento, Rickard, The Many-Electron Energy in Density Functional Theory (2005).
12. K. Capelle, A bird's-eye view of density-functional theory, http://arxiv.org/abs/cond-mat/0211443.
13. Kohn, W. (1995), Density functional theory for systems of very many atoms. Int. J. Quantum Chem., 56: 229-232. https://doiorg.ezproxy.its.uu.se/10.1002/qua.560560407
14. Marques, M. A., Oliveira, M. J. & Burnus, T. Libxc: a library of exchange and correlation functionals for density functional theory. *Comput. Phys. Commun.* **183**, 2272–2281 (2012
15. Borlido, P., Schmidt, J., Huran, A.W. *et al.* Exchange-correlation functionals for band gaps of solids: benchmark, reparametrization and machine learning. *npj Comput Mater* **6,** 96 (2020). https://doi.org/10.1038/s41524-020-00360-0
16. Lehtola, S., Steigemann, C., Oliveira, M. J. & Marques, M. A. Recent developments in libxc—a comprehensive library of functionals for density functional theory. *SoftwareX* **7**, 1–5 (2018).
17. Perdew JP, Burke K, Ernzerhof M. 1995 Generalized gradient approximation made simple. Phys. Rev. Lett. 77, 3865–3868. (doi:10.1103/PhysRevLett.77.3865)
18. Perdew, J. P., Burke, K. & Ernzerhof, M. Erratum: generalized gradient approximation made simple [Phys. Rev. Lett. 77, 3865 (1996)]. *Phys. Rev. Lett.* **78**, 1396–1396 (1997).
19. Becke, A. D. Density-functional thermochemistry. iii. the role of exact exchange. *J. Chem. Phys.* **98**, 5648 (1993).
20. Heyd J, Scuseria GE, Ernzerhof M. Hybrid functionals based on a screened Coulomb potential. *The Journal of chemical physics*. (2003)

21. Heyd J, Scuseria GE. Efficient hybrid density functional calculations in solids: assessment of the Heyd-Scuseria-Ernzerhof screened Coulomb hybrid functional. *The Journal of chemical physics*. (2004)
22. *Becke, Axel D. (2014-05-14). "Perspective: Fifty years of density-functional theory in chemical physics". The Journal of Chemical Physics.* ***140*** *(18): A301.*
23. J. P. Perdew and Y. Wang, Phys. Rev. B **33**, 8800 (1986); https://doi.org/10.1103/PhysRevB.33.8800 J. P. Perdew and Y. Wang
24. Mahdi Davari Esfahani, M., Wang, Z., Oganov, A. R., Dong, H., Zhu, Q., Wang, S., Rakitin, M. S., & Zhou, X. (2016). Superconductivity of novel tin hydrides (SnnHm) under pressure. Scientific Reports, 6(1), 22873. https://doi.org/10.1038/srep22873
25. Mazitov, Arslan & Oganov, Artem. (2021). Evolutionary algorithm for prediction of the atomic structure of two-dimensional materials on substrates.
26. C. W. Glass, A. R. Oganov, N. Hansen, Comput. Phys. Commun. 2006, 175, 713 – 720.
27. W. Tang, E. Sanville, and G. Henkelman A grid-based Bader analysis algorithm without lattice bias, *J. Phys.: Condens. Matter* **21**, 084204 (2009).
28. Alhanash, M. (2021). Effect of Electronic Exchange-Correlation Interaction in the Physics of Ion Insertion in Organic Salts (Dissertation). Retrieved from http://urn.kb.se/resolve?urn=urn:nbn:se:uu:diva-445623
29. Jouhara, Alia, et al. "Raising the Redox Potential in Carboxyphenolate-Based Positive Organic Materials Via Cation Substitution." *Nature Communications*, vol. 9, no. 1, 2018, pp. 4401-11.